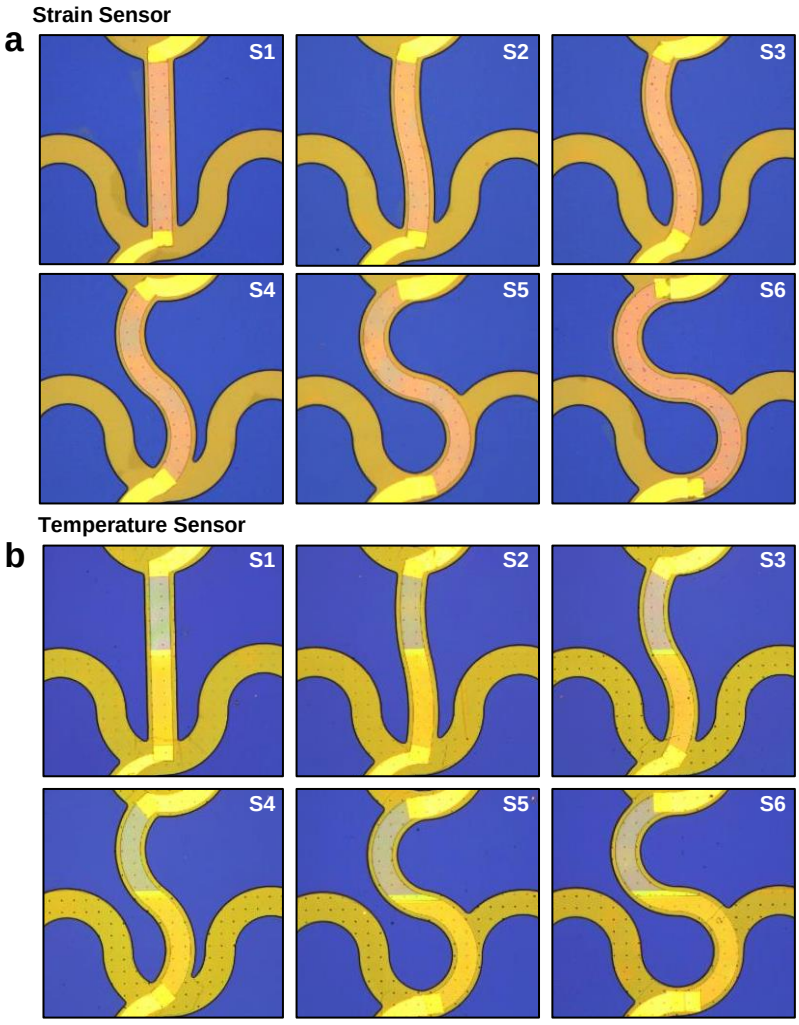

Supplementary Figure 1. Microscope images of the serpentine shaped strain and temperature sensors with various curvatures, κ = 0 (S1), 1.94 (S2), 4.74 (S3), 7.4 (S4), 9.75 (S5), 10 mm^{-1} (S6). **a,** Linear and serpentine shaped p-type doped SiNRs for strain sensors. **b,** Linear and serpentine shaped SiNRs p-n junction diodes for temperature sensors.

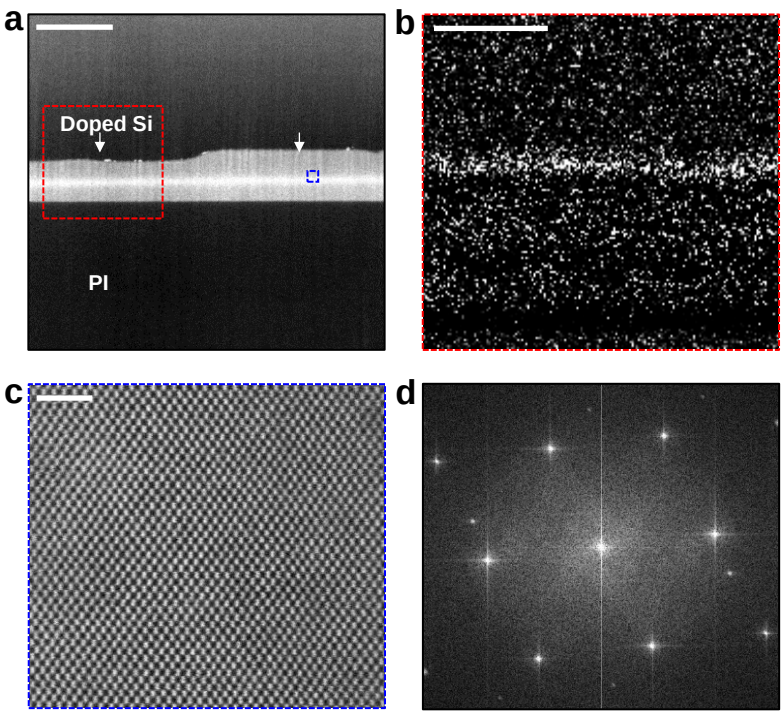

Supplementary Figure 2. Transmission Electron Microscopy (TEM) images of doped single crystalline silicon. **a,** Cross sectional TEM image of p-type doped single crystalline silicon transferred on PI. Scale bar, 200 nm. **b,** Electron Energy Loss Spectroscopy (EELS) map of boron (white dots) at the doped region of the silicon (red dotted box of Fig. S2a). Scale bar, 100 nm. **c,** Magnified TEM image of the single crystalline silicon (blue dotted box of Fig. S2a). Scale bar, 2 nm. **d,** Fast Fourier Transform (FFT) diffraction pattern showing crystallinity of the silicon.

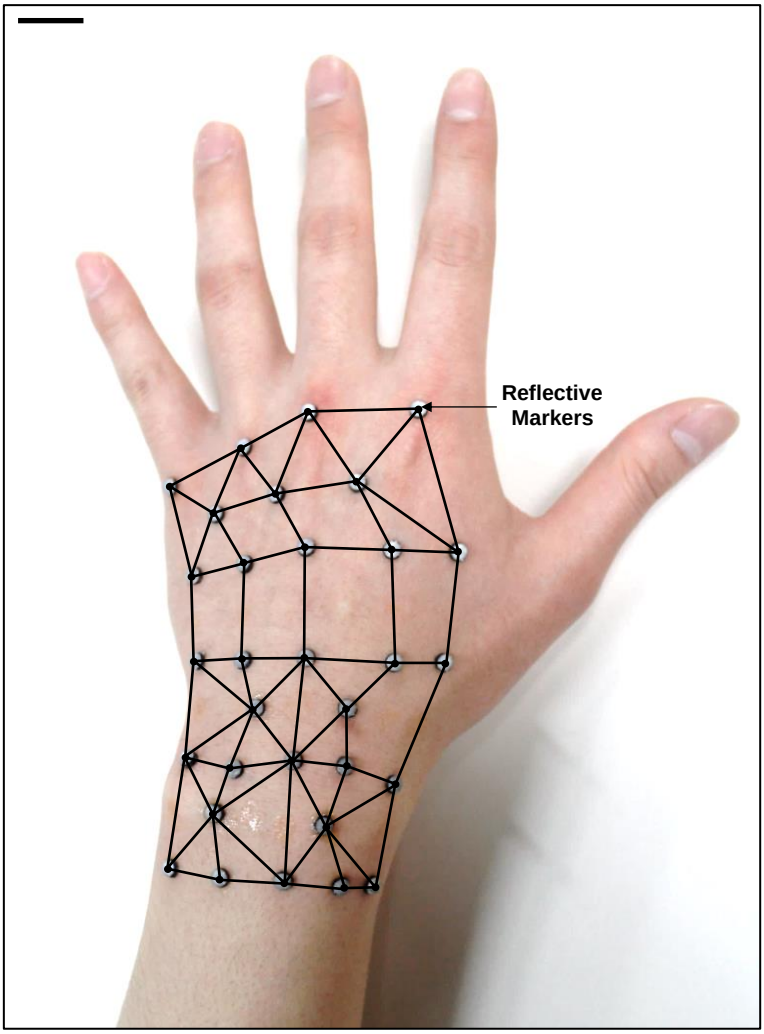

Supplementary Figure 3. Reflective markers for measuring site-specific deformations of the hand skin using motion capture camera system. Lines indicate the distance between adjacent markers for calculating induced strains. Scale bar, 2 cm.

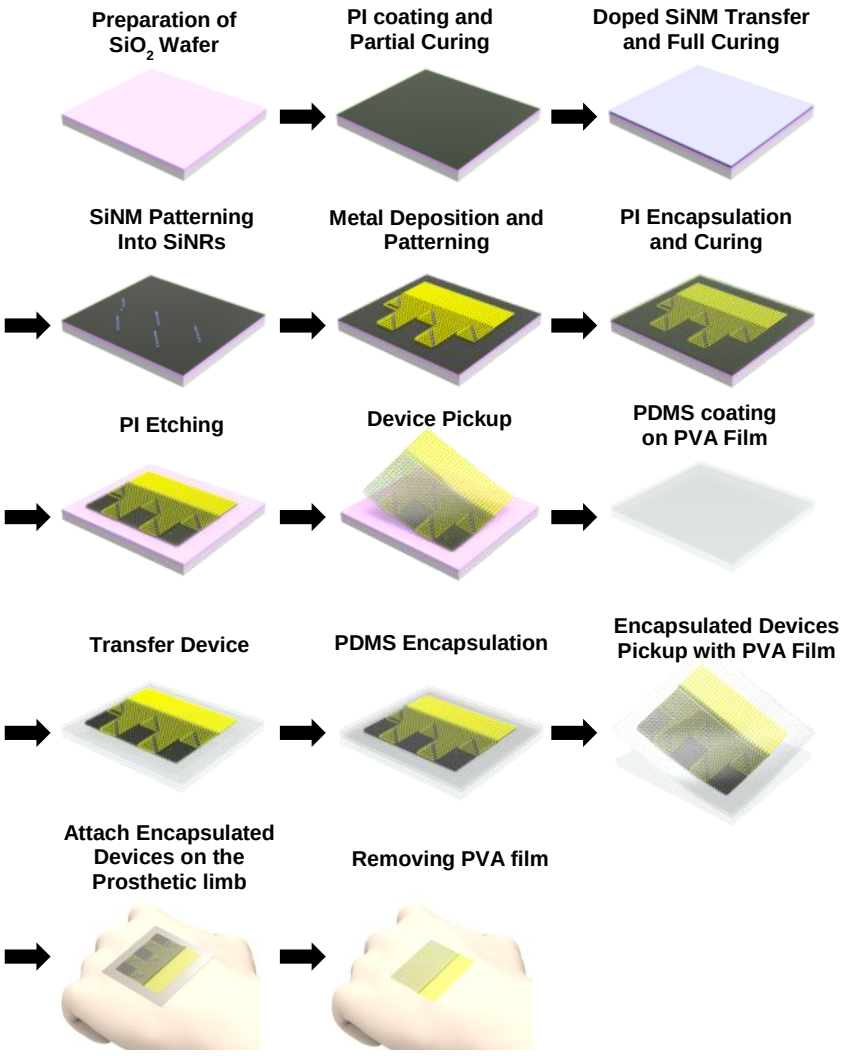

Supplementary Figure 4. Schematic overview of the fabrication process of a SiNR-based sensor array.

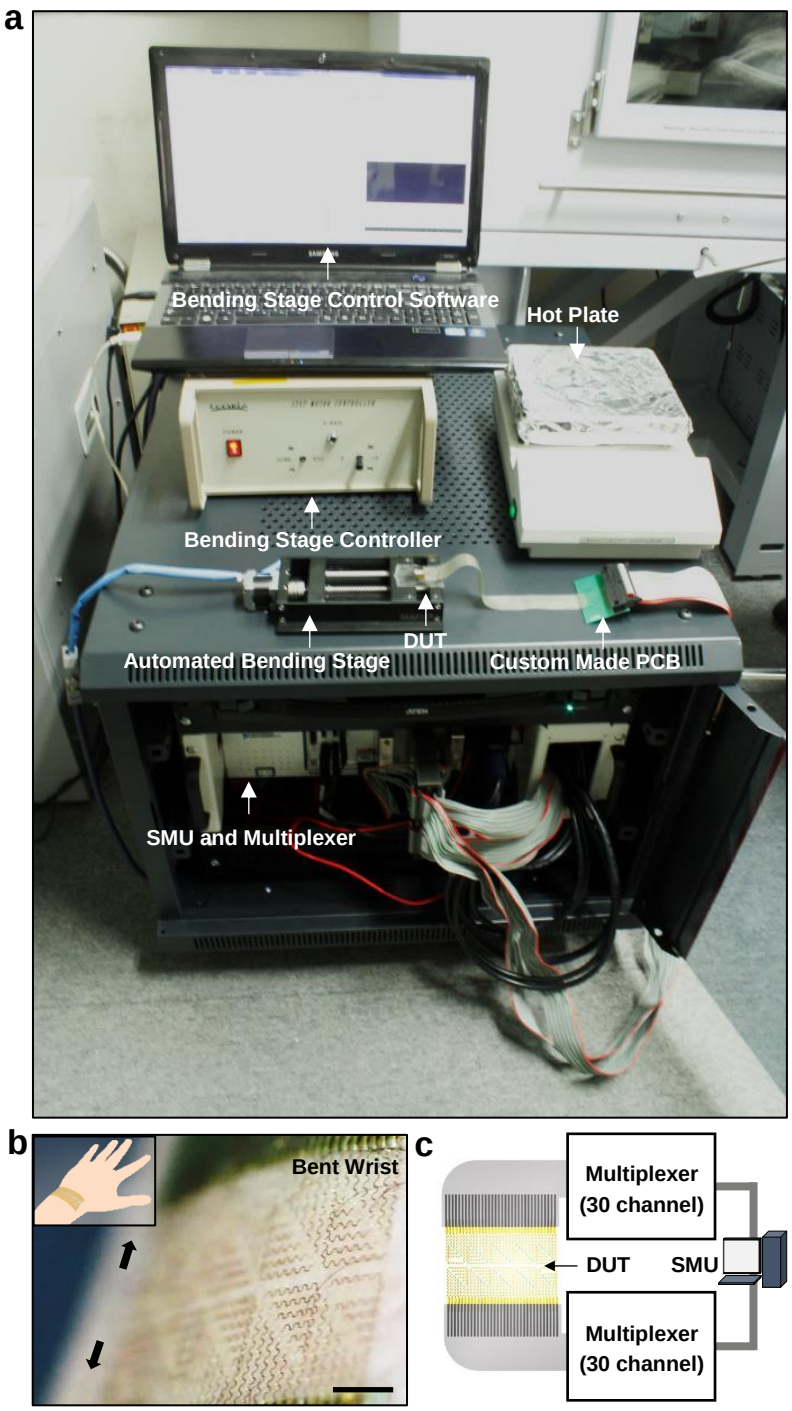

Supplementary Figure 5. Experiment and measurement setup. **a,** Experiment setup to measure the strain and temperature using SiNR-based sensor arrays. **b,** Magnified image of the conformally attached strain gauge arrays on the wrist. Scale bar, 2 mm. Inset shows the corresponding schematic illustration. **c,** Multiplexing schemes for measuring the regional strain distribution with the sensor arrays.

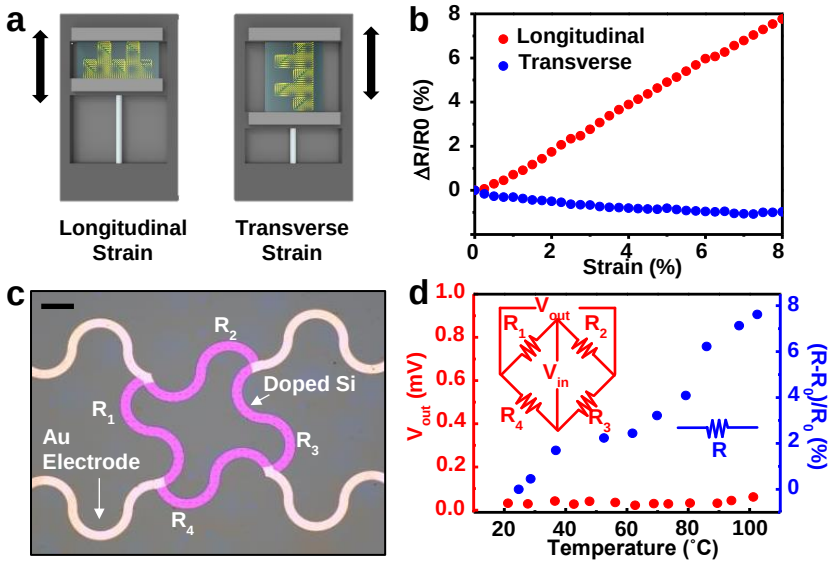

Supplementary Figure 6. a, Illustration of experimental setup for the analysis of stretching directional dependency of the SiNR strain gauge. **b,** Percent resistance changes of a SiNR strain gauge against longitudinal (red) and transverse (blue) strain. **c,** Microscope image of SiNR strain gauges in the Wheatstone bridge configuration. Scale bar, 150 μm. **d,** Output voltage changes measured from the Wheatstone bridge (red) and percent resistance change of single-resistor-based strain gauge (blue) as a function of temperature. Schematic diagram of the Wheatstone bridge (red inset) and single-resistor-based strain gauge (blue inset).

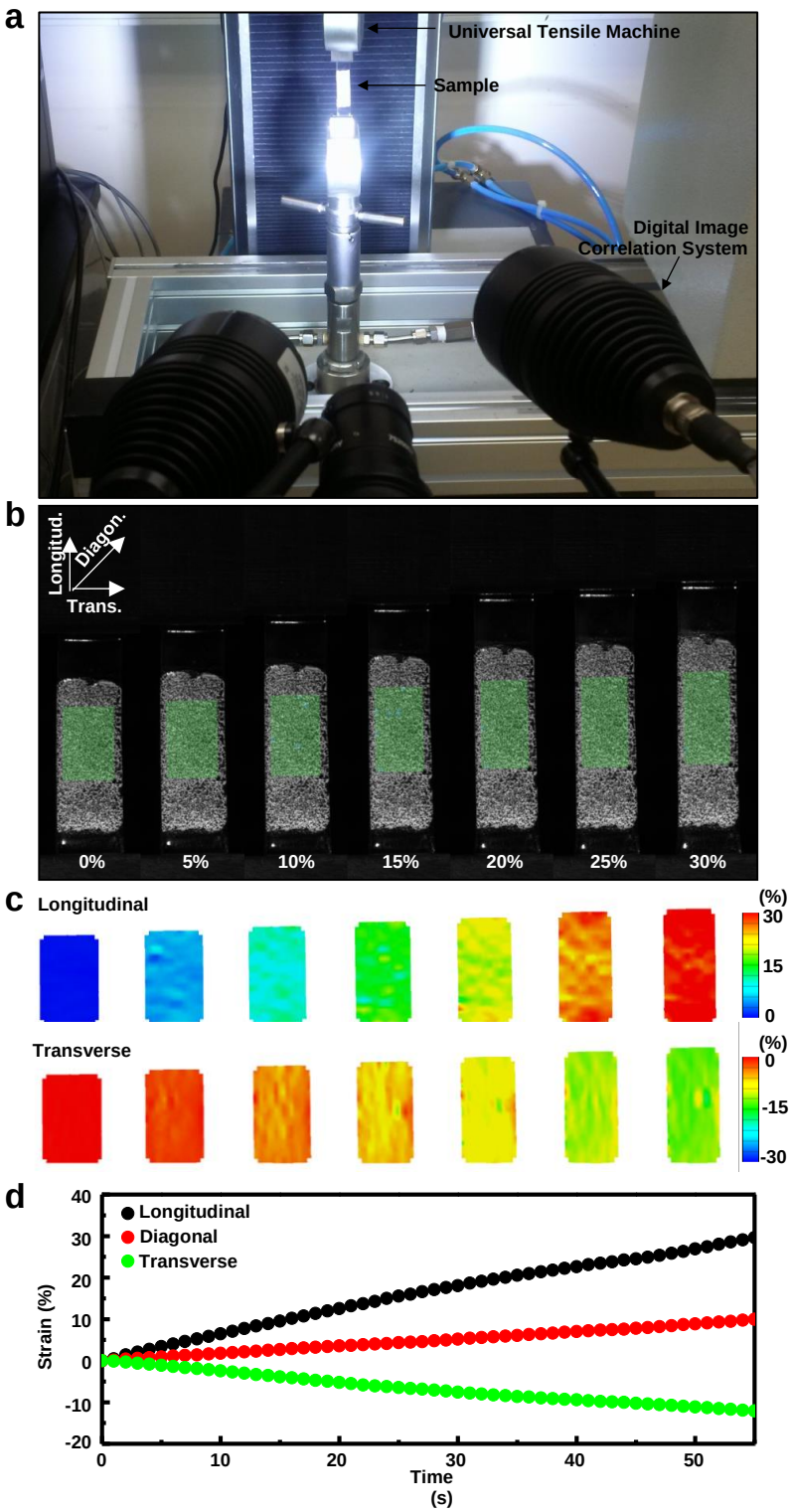

Supplementary Figure 7. a, Photograph of camera-based experimental setup used for analysis of the 2D strain distribution on uniaxially stretched PDMS. **b,** Serial images of the stretched PDMS sample (0~30%). The sample is coated with paint in dot patterns to allow position recognition. Green rectangles in the figure indicate the measured region. **c,** Areal strain distributions in the longitudinal (top) and transverse (bottom) directions of the uniaxially stretched PDMS show changes which can be measured with strain gauge rosettes. **d,** Tri-axial changes in strain as a function of time. The stretching rate is 6 mm min^{-1}.

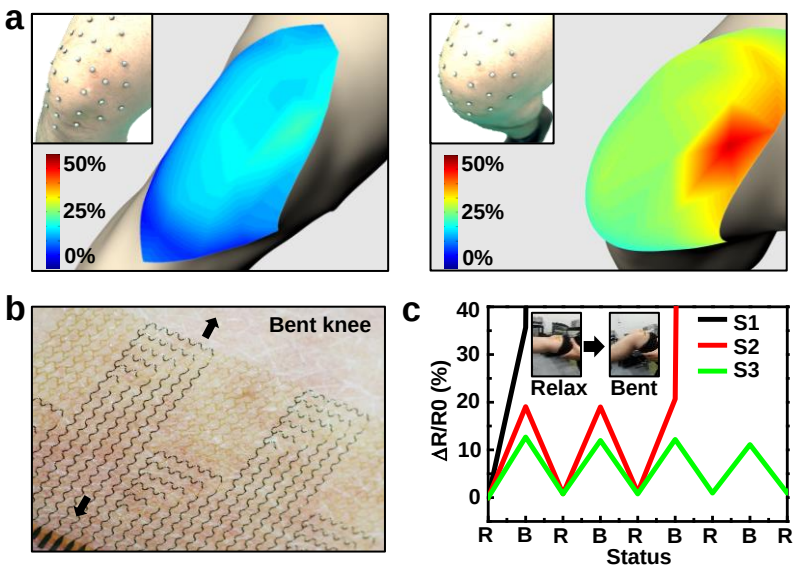

Supplementary Figure 8. Detection of strains at the knee during the bending motion. **a,** Regional strain maps of the skin over the knee, calculated using positional information acquired by the motion capture system, in case of minimal bending (left) and extreme bending (right). Insets show the image of the knee with reflective markers. **b,** Magnified image of the conformally attached strain gauge arrays on the bent knee. **c,** Percent resistance changes of strain gauges with different designs (S1, S2, S3) depending on the motion status (repetitive relaxing and bending of the knee). S1 and S2 designs fail during the cyclic bending motion.

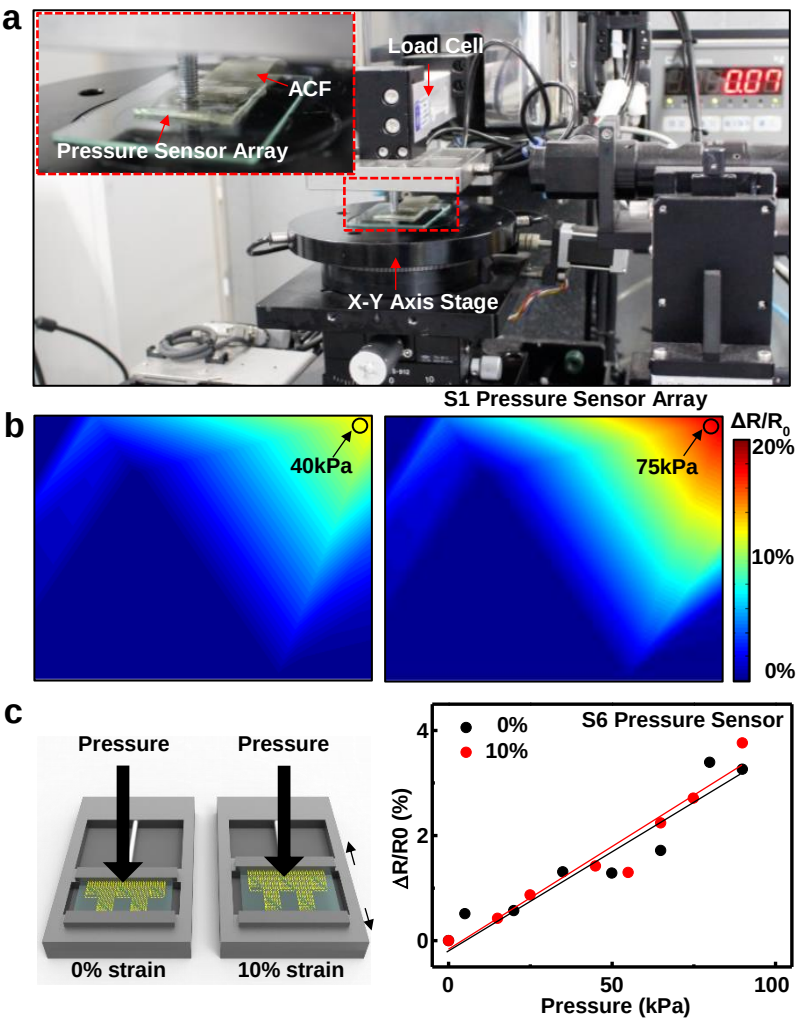

Supplementary Figure 9. a, Experimental setup for SiNR pressure sensor characterization. The pressure sensor array was pressed (inset) and the resistance change of the pressure sensor array was simultaneously monitored. **b,** Percent resistance change maps obtained by using pressure sensor arrays of S1 design for different pressures (40 kPa, 75 kPa). **c,** An illustration of the experimental setup for applying mechanical stimuli on the stretched pressure sensor array (left), and percent resistance change of the S6 pressure sensor design (right) under 0% (black) and 10% (red) strain levels.

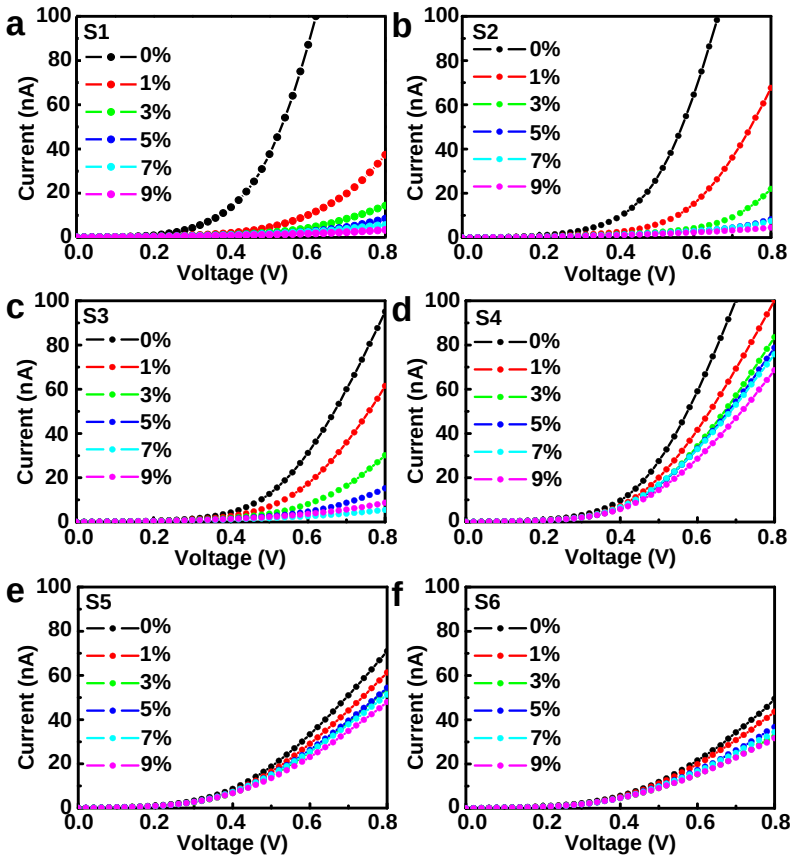

Supplementary Figure 10. I-V characteristic curves of temperature sensors under applied strains (0%, 1%, 3%, 5%, 7%, 9%) at room temperature with different designs: **a,** S1, **b,** S2, **c,** S3, **d,** S4, **e,** S5, **f,** S6.

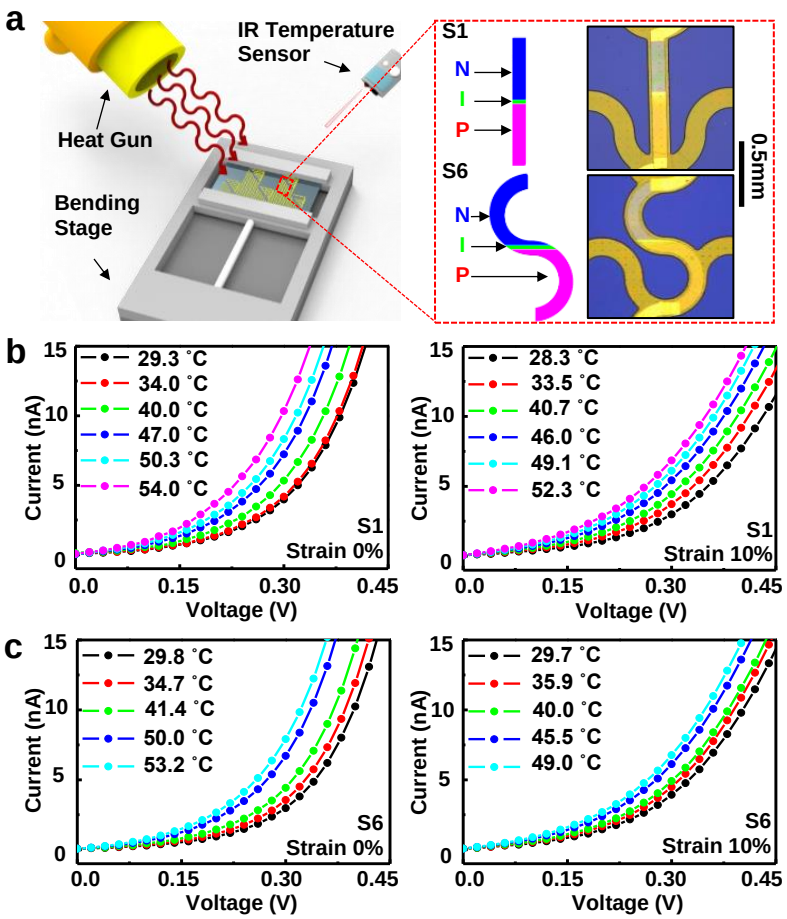

Supplementary Figure 11. Experimental setup and I-V curves of temperature sensors at different temperatures with various applied strains. **a,** Schematic of experimental setup for SiNR temperature sensor characterization. **b,** I-V curves of the S1 temperature sensor without (left) and with applied strain (10%, right). **c,** I-V curves of the S6 temperature sensor without (left) and with applied strain (10%, right).

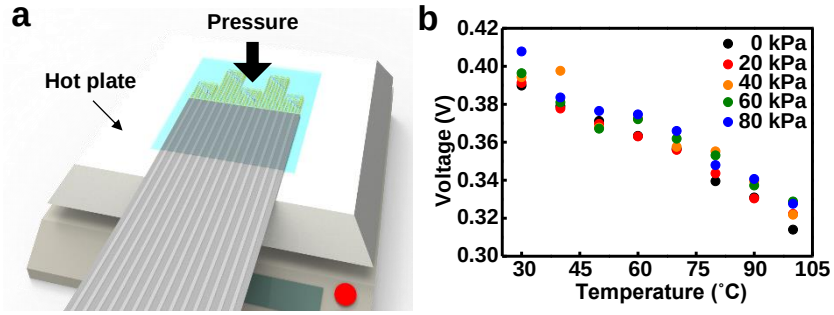

Supplementary Figure 12. a, An illustration of experimental setup for applying pressures to the S6 design temperature sensor array. **b**, Calibration curves of the temperature sensor under various applied pressures, 0 kPa (black), 20 kPa (red), 40 kPa (orange), 60 kPa (green), and 80 kPa (blue). Calibration curves are obtained by extracting voltages from I-V curves at the specific current (1 μA).

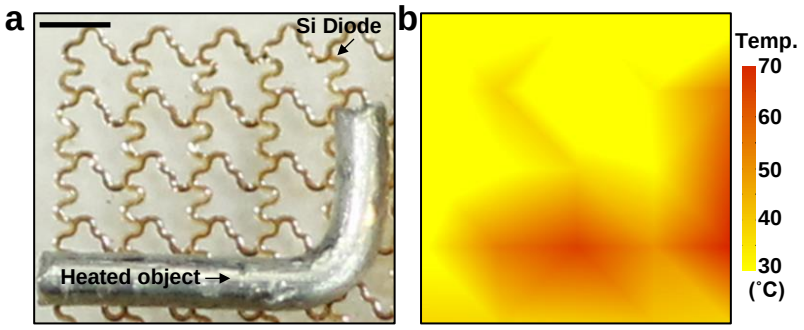

Supplementary Figure 13. Temperature mapping demonstration. **a,** A photograph of SiNRs diode based 5x5 temperature sensor array. Scale bar, 1 mm. **b,** A temperature map obtained by using the temperature sensor array showing a silhouette of the heated object.

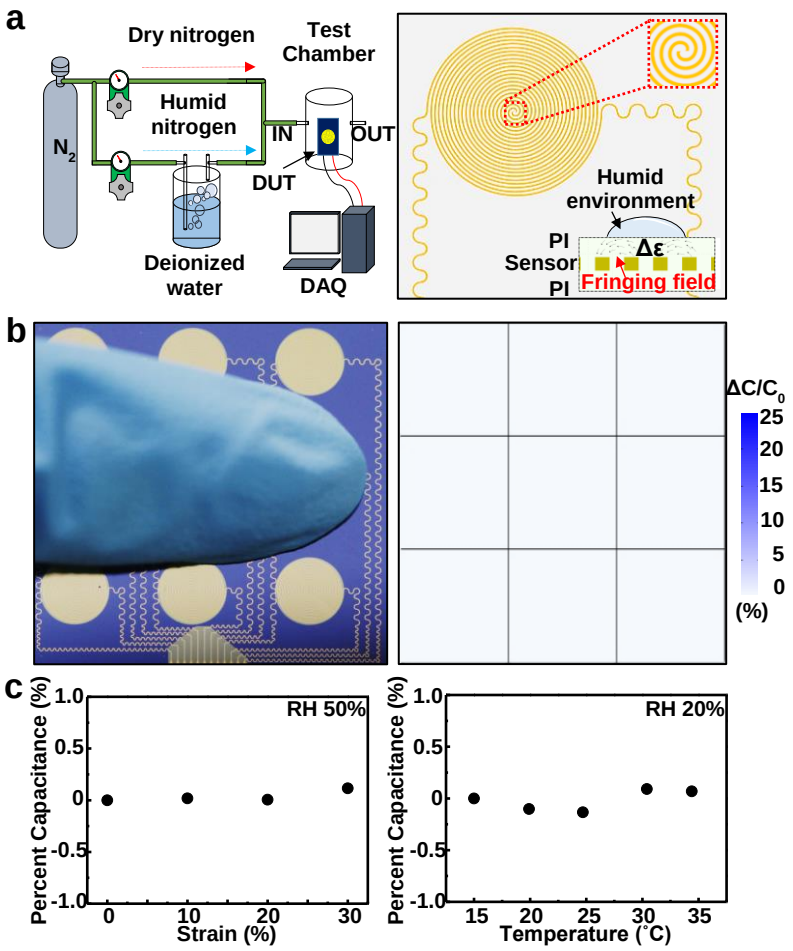

Supplementary Figure 14. a, Illustration of experimental setup (left) and schematic diagram of sensor and sensing mechanism (right) of the humidity sensor. **b,** External disturbance test by touching the humidity sensor array with a dry finger (left) and corresponding responses of the sensor(right). **c,** Strain (left) and temperature (right) dependency of the humidity sensor, measured at the relative humidity (RH) of 50% and 20%, respectively. The humidity sensor shows negligible signal changes against the external strains and temperature changes.

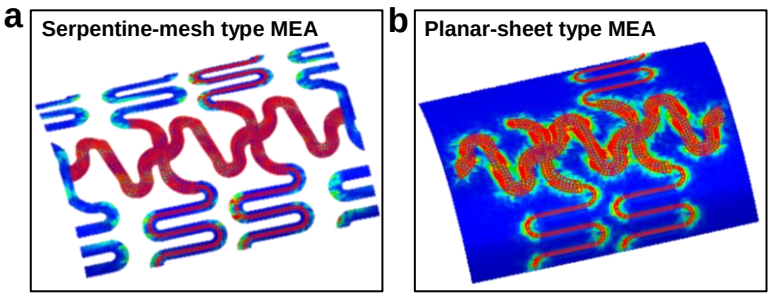

Supplementary Figure 15. FEA mesh highlighting metal interconnections of **a,** serpentine-mesh type MEA and **b,** planar-sheet type MEA.

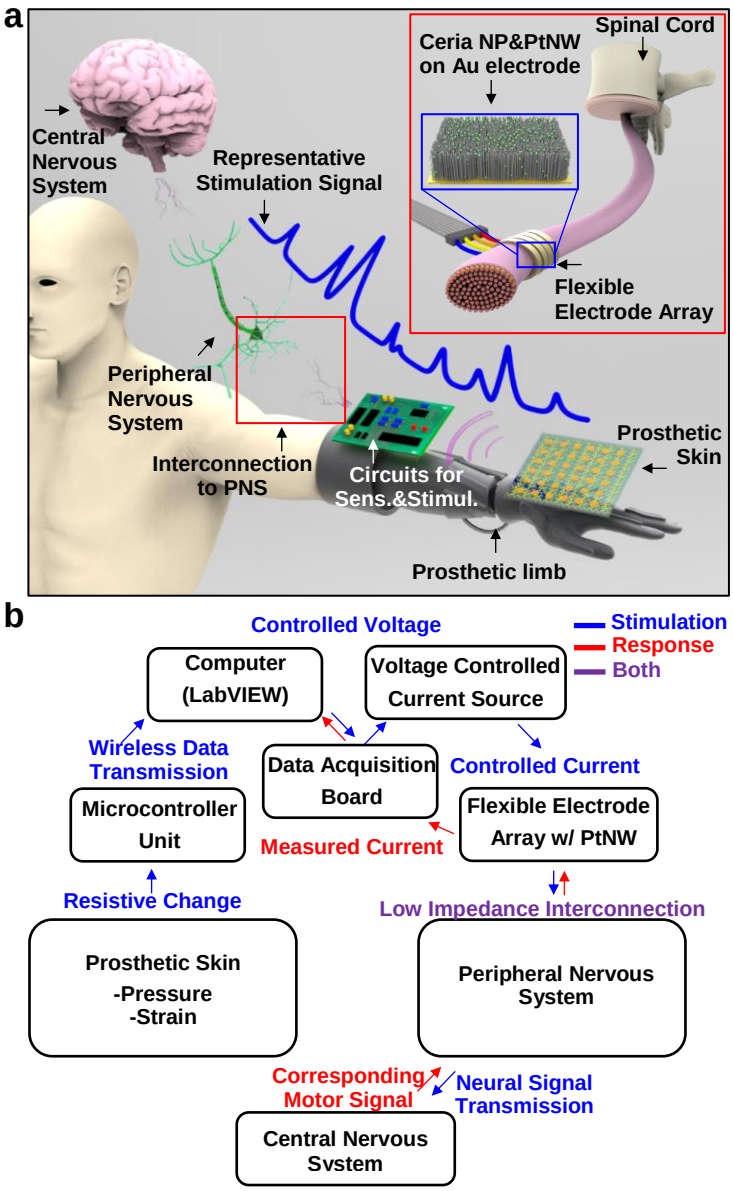

Supplementary Figure 16. a, A conceptual illustration showing necessary components for constructing neural interface to deliver sensed information to the nervous system. **b,** Detailed flow charts describing concept of the bidirectional feedback. Blue, red and purple arrows and descriptions correspond to the case of stimulation, response to the stimulation, and both, respectively.

Supplementary Note 1

Measurement of skin deformations with a motion capture system

A motion capture system is used to measure regional stretchability of skin in the hand and knee regions during various movements. Thirty-one reflective markers (diameter: 3 mm) are attached with ~1.5 cm inter-spacing (Supplementary Fig. 3). The locations and angles of the twelve motion capture cameras (OptiTrack Prime 41, NaturalPoint, USA) are adjusted to optimize signal to noise during the calibration process. The subject wearing reflective markers systematically moves his limbs and motion capture cameras record positional changes of each reflective marker. The recorded data are then analyzed with motion tracking software (Motionbuilder, Autodesk, USA). The amount of skin stretch is estimated by calculating distance changes between nearby reflective markers.

Supplementary Note 2

Finite element analysis (FEA) of SiNR strain gauges

Finite element simulations are used to analyze the strain distribution of SiNR strain gauges during stretching tests (Fig. 3a bottom frames). The SiNR strain gauges with different serpentine designs are modeled using four-node composite shell elements. The strain gauges are embedded between two 60 μm-thick PDMS substrates which are modeled using eight-node solid elements. We assume perfect bonding (no slip condition) between sensors and PDMS substrates. Linear elasticity represents the behavior of the sensor materials. The following anisotropic elasticity parameters are used for single crystalline silicon: $E_{xx} = E_{yy} = 169$ GPa, ν_{xy} =0.064, $G_{xy} = 50.9$ GPa, $G_{xz} = G_{yz} = 79.6$ GPa, where E and ν denote the Young's modulus and the Poisson's ratio, respectively. The *x*- and *y*- axes in Fig. 3a are the <110> directions. The Young's moduli of gold, chromium, and PI are 77.2 GPa, 279 GPa, and 2.5 GPa, respectively. The Poisson's ratios of gold, chromium, and PI are 0.42, 0.21, and 0.34, respectively. The incompressible neo-Hookean model is used to represent the PDMS substrate:

$$W = C_1(I_1 - 3) \quad (1)$$

where W is the strain energy potential, I_1 is the first invariant of the left Cauchy-Green tensor, and C_1 (=18 kPa for PDMS) is a material parameter.

Supplementary Note 3

Strain/pressure mapping using a multiplexer/matrix switch

To measure the resistance changes of dozens of strain gauges/pressure sensors, we use two source

measurement units (SMUs; NI PXIe-4143, National Instruments, USA) that have four channels each and a 128-channel multiplexer/matrix switch (NI PXI-2530B, National Instruments, USA). By using the multiplexer switch, resistances of SiNR strain gauge/pressure sensor arrays are measured sequentially to map regional strain/pressure changes. Six neighboring strain/pressure sensors are grouped and averaged. The complete map of the strain/pressure distribution is obtained by interpolating averaged data over the entire sensing area by using MATLAB software (Mathworks, USA).

Supplementary Note 4

FEA of SiNR pressure sensors

Finite element simulations are used to analyze the strain distribution of SiNR pressure sensors in response to applied external pressures (Fig. 3d right frames). The cross-sections of the SiNR pressure sensors with and without the cavity are modeled using four-node plane-strain elements. The silicon and PI layers are assumed to be bonded perfectly. The pressure boundary conditions (~50 kPa) are applied on the top surface of the PI layer. The linear elasticity that is introduced to simulate SiNR strain gauges is used for silicon and PI.

Supplementary Note 5

Temperature mapping using SiNR temperature sensors

There is an inverse linear relationship between temperature and the resistance of SiNR p-n junction diode temperature sensor, in which the constant current is supplied (500 nA and 5 μA for the temperature map in Fig. 4 and Supplementary Fig. 11b, respectively). Prior to temperature mapping, the temperature sensor is calibrated with a commercial IR camera (i5, FILR, Sweden). During the measurement, SiNR temperature sensors are forward biased by the SMUs and electrical current is sequentially applied to temperature sensors by the multiplexer switch. The resistances of each SiNR temperature sensor are converted into temperatures using the calibration data. Data from six neighboring SiNR temperature sensors are averaged. The averaged data over the entire sensing area are interpolated by the MATLAB software to obtain the temperature map.

Supplementary Note 6

Humidity mapping using humidity sensors

We inject water droplets on the selected regions of the humidity sensor array (Fig. 4d left). The capacitance changes are measured with a digital multimeter. The measured capacitance changes are collected and visualized across multiple sensors (Fig. 4d right) using the MATLAB software.

Supplementary Note 7

Detailed procedures to expose sciatic nerves of a rat

Animal experiments are approved by the animal care committee at Seoul National University Hospital. A Sprague Dawley rat is anesthetized by intraperitoneal injection of ketamine (100 mg kg^{-1}) and xylazine hydrochloride (5 mg kg^{-1}). During the induction of anesthesia, the rat is kept at room temperature, shaved near the buttock area, and placed in prone position. After the skin incision, the gluteus muscles are exposed and dissected until the sciatic nerve is visible.

Supplementary Note 8

FEA of the shear stress distribution at the interface between the stretchable multi-electrode array (MEA) and the nerve fiber

Finite element simulations are used to analyze the shear stress distribution at the interface between the stretchable MEA and a nerve fiber (Fig. 6e right). The MEA is modeled using four-node composite shell elements. The nerve fiber is modeled as a circular cylinder of 1 mm radius using eight-node solid elements. The initially-flat finite element model of MEA is bent to a radius of curvature of 1 mm to be wrapped on the nerve fiber. The MEA and the nerve fiber are attached using the cohesive surface contact and the nerve fiber is stretched axially (5%). The shear stress develops at the interface during stretching to maintain the assumed perfect bonding between the MEA and the nerve fiber. For point of comparison, a flexible, planar-sheet type MEA without serpentine-mesh structure is also modeled. The linear elasticity that is introduced to simulate the SiNR strain gauges is used for gold and PI. The incompressible neo Hookean model is used to represent the nerve fiber with the parameter C_1 of 16.7 kPa.

Supplementary Note 9

Detailed procedures for measuring electrophysiological signals from the rat brain

To simultaneously measure the electrophysiological signals from the rat brain, the electrode is implanted with a stereotaxic apparatus (Kopf Instruments). Evoked potential recordings are obtained with stainless steel electrodes (0.005 in, Plastics One), positioned in ventral posterolateral nucleus (VPL) of the thalamus (AP: –2.3 mm, ML: 3.0 mm, and DV: –6.0 to –7.0 mm; red line in the inset of Fig. 6h) in the right hemisphere. A reference electrode is inserted on the skull above the cerebellum. The electrodes are fixed to the skull with the cyanoacrylate adhesive and the dental acrylic cement. The neural activity is recorded after signals are amplified 1200-fold, band pass-filtered at 0.1-100 Hz, and digitized at a sampling rate of 400 Hz using a digital EEG system (Comet XL, Astro-Med, West Warwick, RI, USA).

Supplementary Note 10

Detailed procedures for the signal delivery to peripheral nervous system

A MEA with PtNWs, which is transfer-printed on the PDMS/PVA film, is placed on the nerve. Then PVA film is dissolved by dropping phosphate-buffered saline (PBS) solution (WELGENE, Republic of Korea) to make conformal contacts between the MEA and nerve (Fig. 6d, e). A pressure sensor array is connected with a capacitor (1 μF) to construct a RC circuit. Changes of RC delay induced by resistance changes of the pressure sensor are calculated by the microcontroller (Arduino pro mini, SparkFun, USA), which is transmitted wirelessly to the laptop via Bluetooth communication. The RC delay changes are converted to the proper voltage signals for the nerve stimulation by the custom-made LabVIEW program (National Instruments, USA). The stimulation voltage is applied by the analog output ports of the DAQ board and delivered to nerves via the stretchable MEA. The flowing current through the nerve is measured from electrodes located away from the stimulation electrode. Temporal current signal changes are recorded using an electrochemical workstation (Fig. 6f, g; CHI660E, CH Instruments, Inc., USA).